Carbon 120 (2017) 137–144

Contents lists available at ScienceDirect

Carbon

journal homepage: www.elsevier.com/locate/carbon

Nanoscale wear of graphene and wear protection by graphene

Borislav Vasić [a, *], Aleksandar Matković [a, 1], Uroš Ralević [a], Milivoj Belić [b], Radoš Gajić [a]

[a] Graphene Laboratory (GLAB) of Center for Solid State Physics and New Materials, Institute of Physics, University of Belgrade, Pregrevica 118, 11080, Belgrade, Serbia
[b] Science Program, Texas A&M University at Qatar, PO Box 23874, Doha, Qatar

ARTICLE INFO

Article history:
Received 25 January 2017
Received in revised form
20 April 2017
Accepted 8 May 2017
Available online 11 May 2017

ABSTRACT

Mechanical stability and wear resistivity of graphene are prerequisite for its applications in nano-mechanical devices. We employ atomic force microscopy based scratching in order to explore the wear of graphene at nanoscale, and the efficiency of graphene for the wear protection of an underlying substrate. We show that the wear of graphene consists of two processes: 1. the plastic deformation for lower normal loads, followed by 2. a sudden tearing of graphene for high enough normal load, with subsequent graphene peeling off from the substrate. The complete progress of the friction during these processes is measured and explained: the friction starts from low values on plastically deformed graphene, then strongly increases for a short time during graphene tearing, and ends up at lower value on uncovered substrate after graphene peeling. Finally, we demonstrate that around 5 nm thick (over ten layers) graphene flakes provide wear protection of the underlying substrate, while thin graphene flakes, around 1 nm thick (single and bilayer), can only enhance the mechanical capacity of the underlying substrate.

1. Introduction

Graphene is atomically thin and flexible conductor [1], with very large stiffness and strength [2], and with good lubricating properties [3]. Therefore, graphene is a promising material for future nano-electromechanical devices such as nano-electromechanical resonators [4,5], piezoresistive sensors [6–9], and nano-electromechanical switches [10,11]. Graphene, as a very stiff material with a low friction, is an excellent choice for the mechanical protection of underlying substrates and nano-objects, including the wear protection and friction reduction [12,13], as well as van der Waals screening [14]. At the same time, graphene is impermeable to standard gases [15], chemically inert and stable, thus allowing protection against oxidation [16] and corrosion [17,18]. Prerequisite for all these graphene applications is a good understanding of its mechanical stability and wear resistivity at nanoscale.

Wear of graphene as well as wear protection by graphene was mainly studied on micro- and macro-scale, on large graphene sheets obtained by the solution processing [13,19], the epitaxial growth on SiC [20,21], or the chemical vapour deposition (CVD) on copper [22]. Although highly relevant for practical applications, these studies did not consider *nanoscale* wear mechanism of monocrystalline graphene. Graphene fracture at nanoscale was investigated using atomic force microscopy (AFM) based nano-indentation experiments in the context of graphene elastic properties [2,23–25], but without considering the graphene wear during sliding. Some of the first insights into nanoscale wear properties of graphene were gained indirectly, as side results of AFM based scratching experiments used for graphene patterning [26–28]. AFM scratching was used to study graphene wear properties by plowing parallel trenches, but only in the regime of graphene plastic deformation, without graphene fracture [29]. Similar methods were employed to explore the influence of wrinkles on wear of CVD graphene [30] and wear initiated from graphene edges [31,32]. Simultaneously, nanoscale wear of graphene was investigated by numerical simulations as well [12,33–37].

So far, the wear protection of underlying substrate was experimentally demonstrated by the solution processed graphene [13,19], where it was shown that wear tracks were more narrow on the graphene protected steel surface. Wear protection by graphene has been already applied for increased endurance and durability of graphene coated AFM probes [38,39] and enhanced mechanical stability of graphene covered macromolecules [40,41]. Meantime,

* Corresponding author.
E-mail address: bvasic@ipb.ac.rs (B. Vasić).
[1] Present address: Institute of Physics, Montanuniversität Leoben, Franz Josef Straße 18, 8700 Leoben, Austria.

http://dx.doi.org/10.1016/j.carbon.2017.05.036
0008-6223/

numerical simulations showed that single layer graphene enhanced the load carrying capacity of the surface during nanoindentation experiments [12], while the wear protection under sliding conditions could be provided by at least two graphene layers [35].

Low shear strength of graphene makes it an excellent ultra-thin solid lubricant [42]. Nanoscale friction of graphene was widely studied on pristine [3,12,43–46], fluorinated [47–50], hydrogenated and oxidized graphene [49], as well as on graphene-oxide [51,52]. It was shown that graphene enables friction reduction compared to surrounding substrate, while the friction can be efficiently controlled either by a proper functionalization or by controlling the number of graphene layers. Still, the friction progress during the contact sliding, during the plastic deformation and especially at the onset of graphene fracture was much less studied. Only an increase of the friction during graphene rupturing has been demonstrated so far [12,19]. Still, many questions regarding graphene wear properties at nanoscale, friction changes during graphene tearing, and graphene efficiency for wear protection have remained open.

We study wear properties of graphene at nanoscale using AFM based scratching and observe two different processes depending on the applied load: 1. plastic deformation of graphene and underlying substrate at lower normal loads, and 2. graphene tearing and subsequent peeling off from the substrate at higher normal loads. The friction between AFM tip and graphene is low on plastically deformed graphene, then it suddenly increases during the tearing, and thereafter it falls down resembling the friction of bare substrate. Finally, we show that the complete wear protection of the underlying substrate is achieved with 4–5 nm thick graphene layers. On the other hand, thin graphene layers, around 1 nm thick, can only increase the mechanical capacity of the underlying substrate, but cannot protect it from wear.

2. Experimental

Graphene samples were produced by the micromechanical exfoliation on silicon wafers with a thin layer of silicon-oxide on top (around 80 nm thick). AFM measurements were done using NT-MDT system NTEGRA Prima. Topographic imaging of graphene flakes before and after AFM based scratching was done in tapping mode. The phase lag of the AFM cantilever oscillations was recorded simultaneously in order to detect changes in a material contrast of investigated samples before and after the scratching.

AFM based scratching experiments were carried out in contact mode with increased normal load necessary to produce desired changes - deformation of graphene and its tearing. Graphene was scratched only once, both in the case of line scratching as well as in the case of scratching of square domains. The scanning velocity during the scratching was the following: 0.3–0.5 μm/*s* in the case of line scratching, and 1.5 μm/*s* in the case of square domain scratching. We did not observe an influence of the scratching velocity in the range 0.4 μm/*s*–3.5 μm/*s* on resulting graphene deformation and tearing as shown in the Supplementary material in Fig. S1. After scratchings, AFM topographic images were recorded in the tapping mode. Both imaging and AFM scratching were performed using diamond coated DCP20 probes from NT-MDT with a typical force constant of 48 N/m and with a typical tip curvature radius of 50–70 nm. These stiff cantilevers with very robust probes enabled both the AFM scratching with high normal loads up to around 20 μN as well as subsequent imaging without probe replacement. Still, in some case when diamond probes could not give clear images due to their wear and/or attached adsorbates, the imaging was performed using NSG01 probes from NT-MDT with much smaller tip curvature radius, typically around 10 nm. All AFM measurements were done at ambient conditions.

The lateral deflection of AFM cantilevers was recorded during AFM based scratching experiments in order to get information about friction between AFM tip and sample. The friction signal was calculated as the average of the difference between the lateral force signal in the forward and backward direction. Opposite to the topographic images recorded after the corresponding scratching, the presented friction maps were measured during the scratching.

Calibration of the normal force was done by force-distance measurements on hard substrate such as bare SiO_2. The normal force was then calculated as $F_N = kd$, where k is the force constant of employed DCP20 probes, and d is the displacement of the piezo-scanner for the given set-point. Calibration of the lateral force was done using the simple procedure given in Ref. [53].

For studies on wear protection by graphene films, AFM scratching both on bare and graphene covered SiO_2 substrate was done with the same normal load in order to enable straightforward comparison between these two cases. Here we considered the protection of SiO_2 since it allows a straightforward visualization of the flakes, and does not require any additional transfer steps after the exfoliation. Still, the employed method and obtained results can be applied for technologically more relevant materials on which graphene can be either directly grown or transferred, although in that case, grain boundaries and wrinkles in graphene influence its wear properties [30]. Two different cases were explored in the context of wear protection by graphene: 1. the protection by thin graphene layers, with the thickness of around 1 nm corresponding to single or bilayer graphene, and 2. the protection by thicker graphene films, with the thickness of several nanometers, between 3 nm and 5 nm, corresponding to around 10–15 graphene layers.

Raman imaging of graphene was carried out on NTEGRA Spectra confocal Raman system (NA 0.7) with approximately 1 μm spatial resolution. The excitation source was a green laser ($\lambda = 532$ nm).

3. Wear of graphene during AFM scratching

The study on wear properties of graphene we start with AFM scratching of parallel trenches in graphene/SiO_2 substrate. Corresponding topography and phase contrast images obtained with increasing normal load F_N (from 1.41 μN to 17.48 μN) are shown in Fig. 1 (a) and 1(b), respectively. Two selected cross sections are depicted in Fig. 1(c), and the change of the trench depth is given in Fig. 1(d). The trench depth increases with F_N, but there are two distinct processes. In the first one, for the normal loads below approximately 10 μN, graphene is only strained and plastically deformed. In the topographic image, plowed trenches from 1 to 8 are only slightly darker, but without any bumps and cracks. At the same time, the corresponding phase signal is similar to surrounding flat graphene implying there is no material contrast between them. On the other hand, for the normal loads above approximately 11 μN, graphene is cut and torn in an uncontrolled manner, leaving large bumps (bright spots in Fig. 1(a)) near trenches from 9 to 12. In the phase image in Fig. 1(b), trenches 9–12 are dark, with the same contrast as neighboring SiO_2 substrate, confirming that graphene is peeled off, leaving bare and scratched SiO_2 substrate. Typical plateau with uncovered SiO_2 substrate left after the tearing and peeling of graphene is more emphasized with encircled area in enlarged image of trench 12 in Fig. 1(e), as well as in the corresponding cross section along dotted line (SiO_2 plateau is represented with the drop in the height profile on the left side, between the graphene and the trench).

Further insights into graphene wear properties are obtained by AFM scratching of finite domains, not only along single line. Fig. 2 depicts the results for such an example where six square domains (with size 1.5×1.5 μm^2) were plowed for increasing normal load F_N

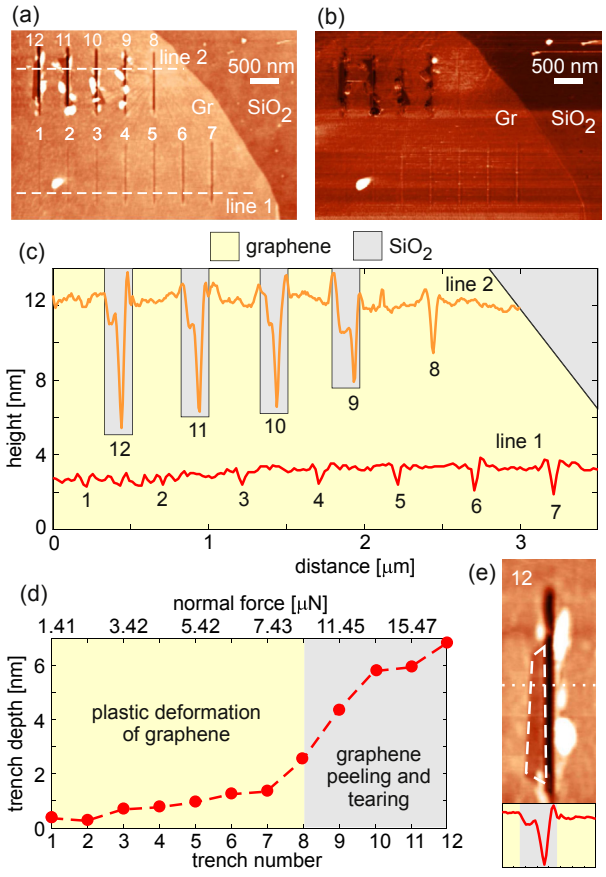

Fig. 1. AFM scratching of graphene along discrete array of parallel lines with increasing normal load F_N = 1.41 μN, 2.41 μN, 3.42 μN, 4.42 μN, 5.42 μN, 6.43 μN, 7.43 μN, 9.44 μN, 11.45 μN, 13.46 μN, 15.47 μN, 17.48 μN: (a) topography, (b) phase image, (c) cross sections along two dashed lines denoted in part (a), (d) depth of the trenches derived from data in part (c), and (e) enlarged topographic images (image width is 500 nm) of trench 12 with the cross section along dotted line whereas the dashed line encircles region where graphene was peeled off leaving bare SiO_2 substrate. Thickness of the graphene flake is around 1 nm. (A colour version of this figure can be viewed online.)

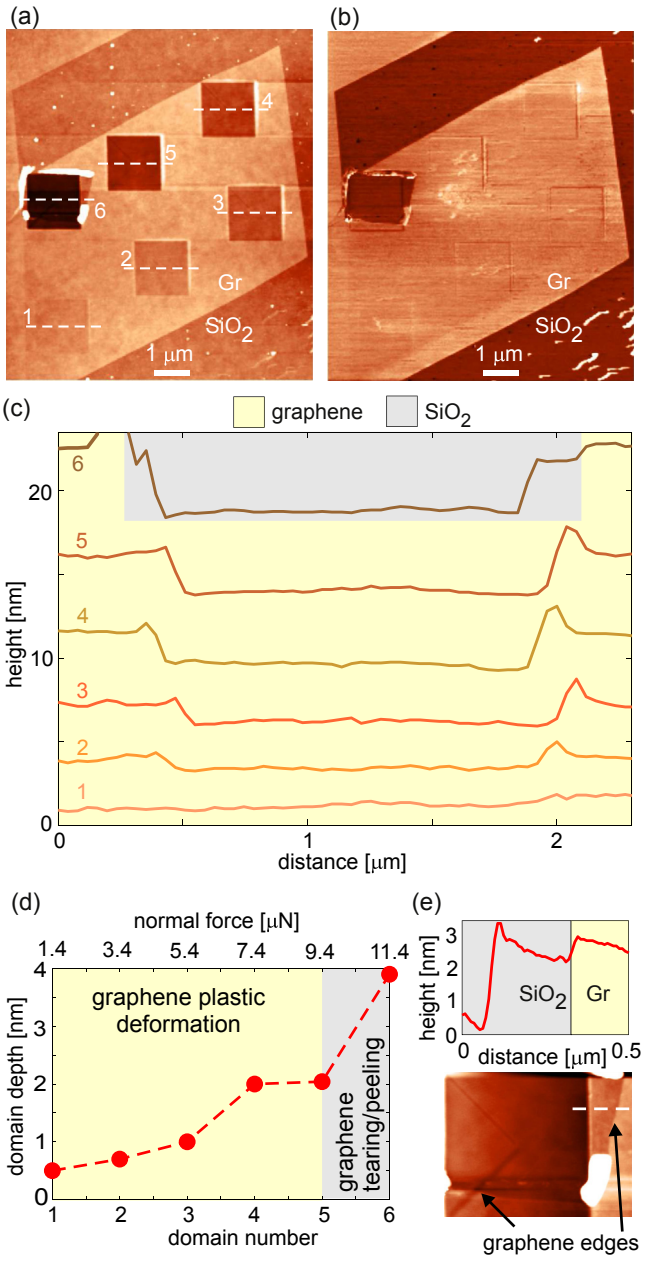

Fig. 2. AFM scratching of graphene within six square domains with increasing normal load F_N = 1.41 μN, 3.42 μN, 5.42 μN, 7.43 μN, 9.44 μN, 11.45 μN: (a) topography, (b) phase image, (c) cross sections along six dashed lines denoted in part (a), (d) depth of the domains, and (e) enlarged topographic image of domain 6 with given cross section along dashed line. Graphene thickness is around 0.9 nm. (A colour version of this figure can be viewed online.)

(from 1.41 μN to 11.45 μN). Plowing of all square domains was done row by row, from bottom to top of every domain, with slightly reduced resolution of 128 × 128 points. Topography and the corresponding phase contrast image are given in Fig. 2(a) and (b), respectively. Cross sections along all six domains are shown in Fig. 2(c), whereas their depth is given in Fig. 2(d). The depth of plowed domains increases with normal load, and again, there are two distinct processes. Within the first five domains, where F_N < 10 μN, graphene is just plastically deformed, without cracks and bumps. The phase image, where these domains have the same contrast as surrounding non-scratched graphene, confirms the material homogeneity. On the other hand, within the sixth domain scratched with F_N = 11.45 μN, graphene is torn and then peeled off from SiO_2 substrate. The phase contrast for this domain is different than the rest of graphene flake, but the same as SiO_2 substrate. Enlarged sixth domain after scratching is shown in 2(e). The arrows show the exact positions of graphene edges after tearing, the large bright spot is a bump produced due to graphene peeling, while the bare SiO_2 plateau is clearly visible in the corresponding cross section.

In both examples, graphene is only plastically deformed for F_N < 10 μN, and fractured at higher applied force. Two additional examples of graphene deformation and fracture are given in the Supplementary material in Figs. S2 and S3. They show the same two processes, while graphene tearing starts for similar normal loads. Plastic deformation of graphene inevitably results in defects, either various vacancy defects such as mono- and di-vacancies, and Stone-Wale defects [54–57], or sp^3 like defects due to rehybridizations [58]. Defects deteriorate graphene mechanical properties. While the elasticity can be still comparable to the elasticity of pristine graphene [23–25], the breaking strength of defective graphene is more decreased, especially in the vacancy-defect regime [59]. In the considered AFM scratching, number of defects in graphene increases with a degree of the plastic deformation, that is, with trench depth. For high enough normal load, graphene becomes so defective, that its breaking strength significantly falls down, leading to

graphene fracture, tearing and finally to uncontrolled peeling along selected path of AFM probe. However, the imaging of atomic defects in graphene is not possible with AFM operating in tapping mode and especially with a large curvature radius of DCP20 probes employed in this study.

In order to further characterize graphene after the scratching, we employed Raman spectroscopy. Obtained spatial maps of Raman modes of the graphene are shown in Fig. S4 of the Supplementary material (Raman imaging was done on the same sample area as in Fig. 2(a) where the scratching of square domains were carried out). As can be seen from the absence of the defect band (D) at around 1350 cm^{-1}, and relative intensities of 2D (around 2686 cm^{-1}) and G (around 1586 cm^{-1}) modes of graphene, the AFM scratching does not introduce defects in the graphene lattice within flat parts of squared domains. On the other hand, defects obviously appear only along deformed graphene, such as scratched trenches or edges of square domains. Still, in order to confirm presence of these defects along such narrow areas (their width is below 100 nm), it is necessary to use tip enhanced Raman spectroscopy, since the spatial resolution of confocal Raman setups is diffraction limited.

Wear of the exfoliated graphene was initiated for the normal loads larger than around 10 μN. In the previous studies, we showed that the wear initiated from wrinkles in CVD graphene [30] and graphene edges [31] started for one and two orders of magnitude lower normal loads, respectively (for the loads below 0.1 μN and around 1 μN, respectively). Therefore, homogeneous graphene, without cracks, exposed edges, and out-of-plane deformations such as wrinkles, can sustain much larger normal loads, and only such graphene is a promising material for protective coatings.

4. Friction during AFM scratching

Applications of graphene as nanoscale lubricant are based on its ability to lower friction of underlying substrate. Still, an opened question is the change of graphene lubricating properties under high normal loads causing graphene wear. In order to explain these changes, we consider the friction evolution during above discussed AFM scratching experiments. Friction maps for all square domains from Fig. 2 were obtained according to recorded lateral force during AFM scratching. Two representative maps are given in Fig. 3(a) and (b) for the fifth and sixth domain, respectively. The friction in Fig. 3(a) is rather homogeneous since graphene is only plastically deformed. On the other hand, the map in Fig. 3(b) consists of three distinct regions with characteristic cross sections given in Fig. 3(c). Dark region, with the cross section along line 1, corresponds to low friction when graphene is just plastically deformed. Sudden increase of the friction due to graphene tearing is visible as a narrow and bright contrast in Fig. 3(b), with the cross section along line 2 in Fig. 3(c). The position of line 2 corresponds exactly to newly formed graphene edge recorded after the scratching shown in Fig. 2(e). Finally, after the initial graphene tearing and peeling along line 2, AFM tip slides along bare SiO_2 substrate and occasionally, further pushes free graphene edges towards the edges of the square scan range. Here, the friction has some intermediate value (the cross section is given along line 1 in Fig. 3(c)) which mainly corresponds to the friction on bare SiO_2.

Fig. 3(d) summarizes the change of the friction for all scratched domains as a function of the normal force. As can be seen, the friction is low as long as graphene covers the underlying substrate. Although low, this friction is non-negligible. Generally, the friction on graphene during AFM imaging increases due to the puckering effect, where due to low bending rigidity of graphene, it easily deforms in the out of plane direction leading to increased contact area with AFM tip [43]. In the case of AFM scratching, due to large

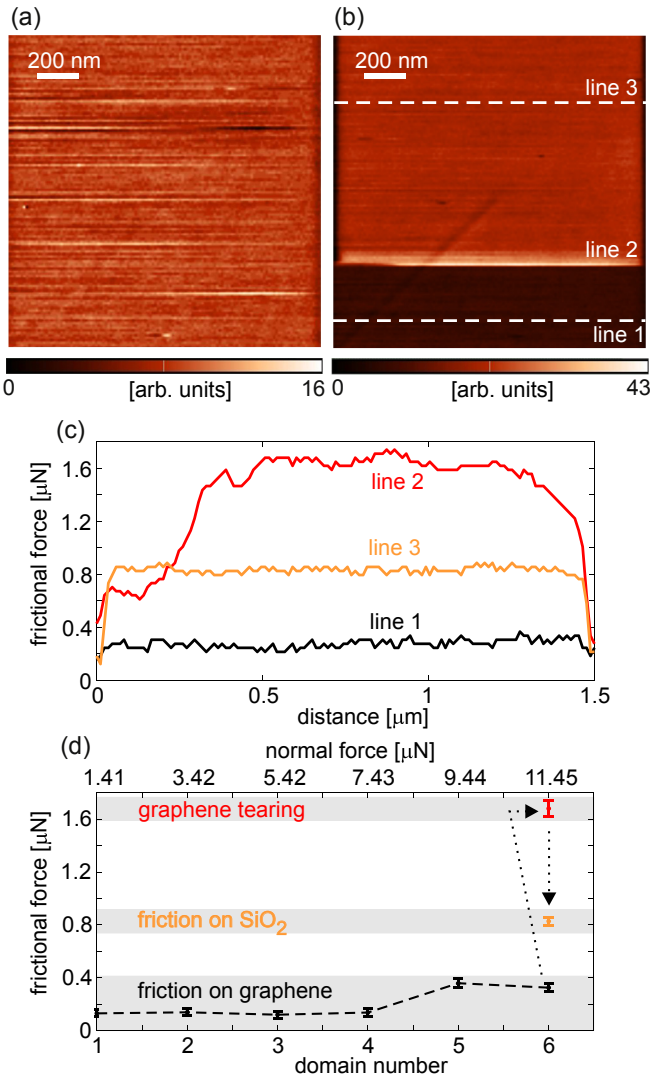

Fig. 3. Friction during AFM scratching of square domains from Fig. 2(a). Friction map during AFM scratching of: (a) the fifth domain, the normal force is F_N = 9.44 μN, whereas graphene is just plastically deformed, (b) the sixth domain, the normal force is F_N = 11.45 μN, whereas graphene is torn and peeled off. (c) Three characteristic cross sections of the friction map in part (b): line 1 stands for the friction on graphene, line 2 is the friction signal during graphene tearing, and line 3 corresponds to the friction on SiO_2 substrate after removing graphene. (d) Average friction on all square domains from Fig. 2(a) as a function on normal load. (A colour version of this figure can be viewed online.)

applied normal loads and significant plastic deformations of graphene, the contact area between graphene and AFM tip is significantly increased compared to common AFM imaging, leading to enhanced friction. During the graphene tearing, the friction force is increased due to additional work needed for graphene tearing and peeling from the substrate. We observed similar increase of the friction force during AFM based lateral manipulation of graphene edges [31]. The same changes of the friction force during scratching of graphene, with the same three typical processes, were observed in other cases as well, and these results are shown in Fig. S5 of the Supplementary material.

5. Wear protection by graphene during AFM scratching

The final goal we would like to address in this study is possible wear protection of materials by covering them with graphene. The

results for the protection with thin graphene films (around 1 nm thick) are summarized in Fig. 4, for the scratching of square domains (increasing normal load from bottom to top row, while domains in the same row were scratched for the same normal load). For the first two rows of square domains (from the bottom) in Fig. 4(a1), the domain depth is lower on graphene covered SiO_2 substrate by around 2 nm as can be seen from the characteristic cross sections in Fig. 4(a3). Therefore, thin graphene flakes can not provide wear protection of underlying substrate since in both bare and graphene covered SiO_2 are plastically deformed. Still, the thin graphene flakes can improve the mechanical load capacity of an underlying substrate by decreasing the wear depth of the underlying SiO_2.

For high enough normal load, graphene is torn and peeled off from the substrate in the third (top) domain in Fig. 4(a1). This is confirmed by different phase contrast in Fig. 4(a2). Obviously, in this case, there is no possibility for any protection by graphene, and the resulting wear depth is even increased compared to bare substrate as can be seen from the corresponding cross section in Fig. 4(a3) along line 3. In some cases, we did not observe any improvement of the load capacity as shown in the third example in Fig. 4(b). Here graphene is just plastically deformed in whole range of applied normal loads, but the depth of scratched domains is similar both on bare and graphene covered substrate (in some cases even larger in the latter case as shown for line 1 in Fig. 4(b2)). The observed absence of the improved load capacity is probably due to continuous changes in AFM tip shape during plowing, so that the same normal force produce different stress, or due to local changes in graphene-substrate adhesion which can strongly influence both graphene plastic deformation as well as tearing [33,34].

Possible way to improve wear protection is to use thicker flakes consisting of more graphene layers. Two such examples are depicted in Fig. 5 showing the topography recorded after AFM scratching of square domains with increasing normal load. In both cases, around 4.5 nm thick graphene provides excellent wear protection since the graphene surface stays practically intact (small protrusions on graphene film in part (b) probably originate from AFM tip during scratching, since their shape changes from scan to scan). On the other hand, the same normal loads produce several nanometer deep square domains on bare SiO_2. Additional results given in the Supplementary material in Figs. S6 and S7 confirm the previous conclusions. Furthermore, they show that exposed graphene edges in the top graphene layer of a multi-layer graphene flakes are always weak points in the wear protection.

However, even thicker graphene flakes can not provide perfect protection if the normal load is above certain threshold. Results for this case and AFM scratching along parallel lines are shown in Fig. 6. In the first two cases in parts (a) and (b), the normal loads for AFM scratching was $F_N = 8.63$ μN and $F_N = 10.39$ μN, respectively. As can be seen, 4 nm thick graphene flakes give practically perfect wear protection of SiO_2 substrate. From the topographic images in Fig. 6(a1) and 6(b1), trenches are clearly visible on SiO_2 surface, while they can be hardly recognized on graphene (there are only slightly darker shadows compared to the rest of graphene flakes marked by the arrows along which graphene was scratched). As can be seen from the corresponding cross sections in Fig. 6(a2) and 6(b2), while the depth of trenches on bare SiO_2 substrate is around 1–2 nm, the graphene surface is almost flat, with slightly increased surface roughness only. In the last case, the normal load was further increased to $F_N = 12.15$ μN. The results in Fig. 6(c1) and 6(c2) show that the graphene perfectly protects underlying SiO_2 substrate along the first and part of the second scratched line (counted from the left, scratching was done from the top to the bottom) as in the previous cases. Suddenly, graphene flake is locally torn and removed from the substrate. In subsequent lines, graphene is either only removed from the substrate, or it is removed, and the uncovered substrate is then further plowed as in the case of bare SiO_2.

Distribution of the normalized wear depth d as a function of the normalized applied normal load f for all above discussed results is given in Fig. 7. Normalized force is calculated as $f = F_N/F_{N,\max}$ where

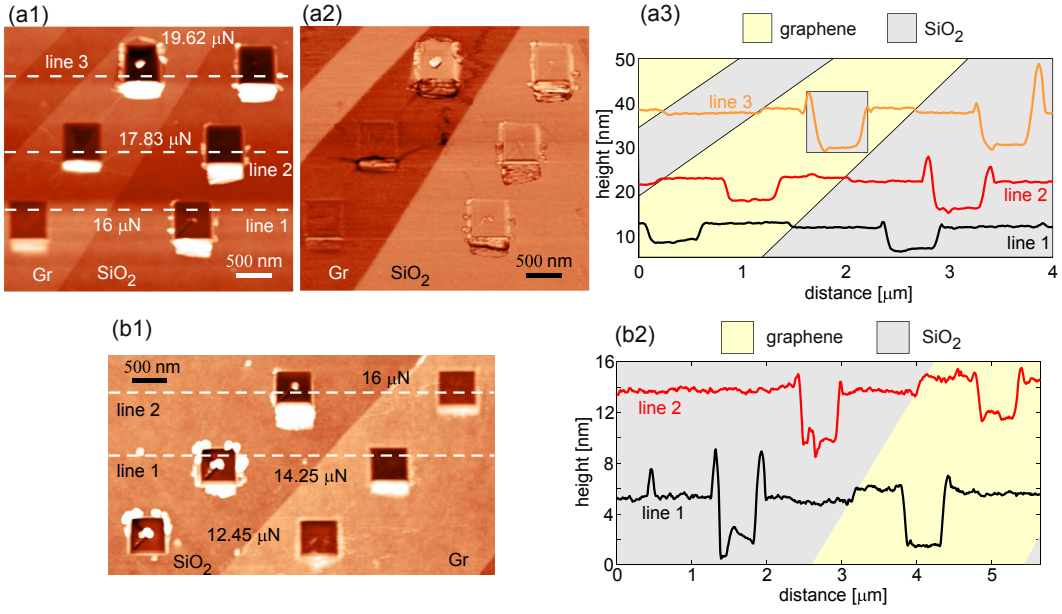

Fig. 4. Wear protection by thin graphene flakes: (a1) topography of square domains after AFM scratching, (a2) corresponding phase image, (a3) cross sections along the dashed lines denoted in part (a1); (b1) topography after AFM scratching of square domains, (b2) cross sections along the dashed lines denoted in part (b1). Thickness of the graphene flake is around 0.8 nm for part (a) and 1 nm for part (b). Normal forces used for AFM scratching were the following: (a) $F_N = 16$ μN for the bottom row, $F_N = 17.83$ μN for the middle row, and $F_N = 19.62$ μN for the top row of square domains, (b) $F_N = 12.45$ μN for the bottom row, $F_N = 14.25$ μN for the middle row, and $F_N = 16$ μN for the top row of square domains. Therefore, the normal load was increased from bottom to top row, while the domains in the same row (one on bare SiO_2, the other one on graphene covered SiO_2 substrate) were scratched for the same normal load. (A colour version of this figure can be viewed online.)

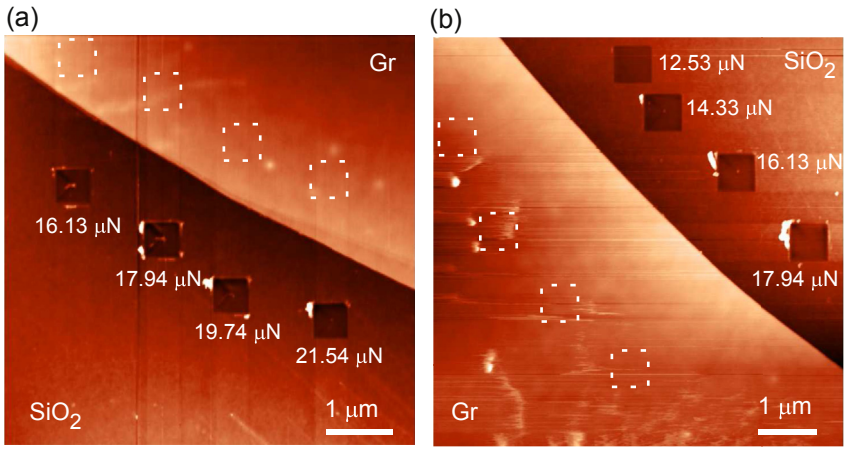

Fig. 5. Wear protection by thick graphene flakes for the case of AFM scratching of square domains: both parts (a) and (b) show the topography recorded after the AFM scratching (z-scale is 10 nm in both images). The normal force for the scratching is the following: (a) for domains from left to right $F_N = 16.13$ μN, 17.94 μN, 19.74 μN, 21.54 μN, (b) for domains from left to right $F_N = 12.53$ μN, 14.33 μN, 16.13 μN, 17.94 μN. Thickness of the graphene flakes is around 4.5 nm in both cases. Regions for AFM scratching on graphene are denoted with square domains (dashed lines). (A colour version of this figure can be viewed online.)

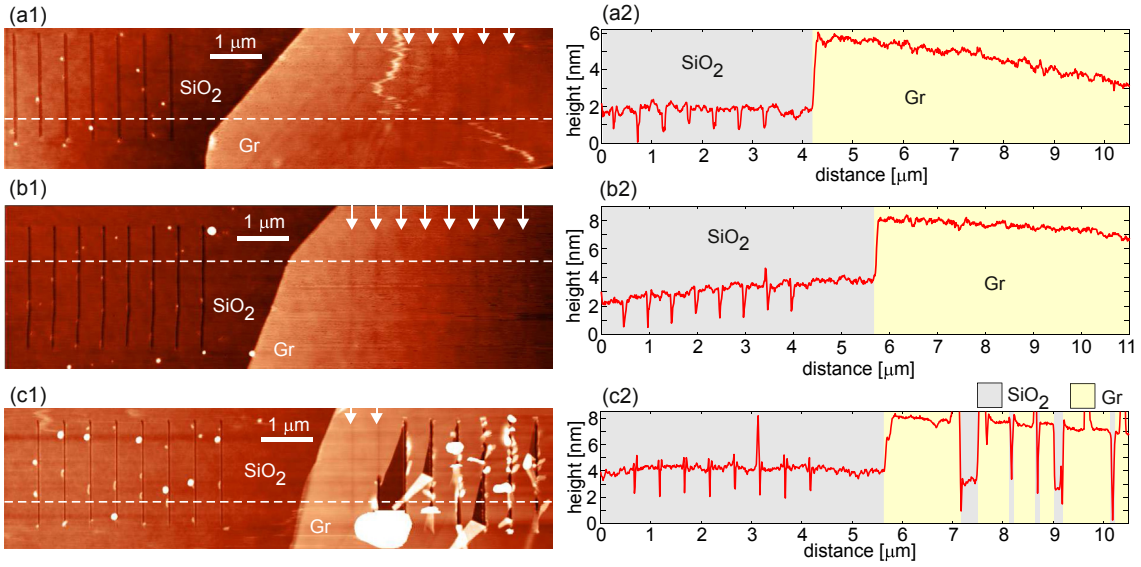

Fig. 6. Wear protection by thick graphene flakes for the case of AFM scratching along parallel lines: (a1-b1-c1) topography and (a2-b2-c2) cross sections along the selected dashed lines in parts (a1-b1-c1). Normal forces used for AFM scratching were the following: (a) $F_N = 8.63$ μN, (b) $F_N = 10.39$ μN, and (c) $F_N = 12.15$ μN. Thickness of the graphene flake is around 4 nm. White arrows in parts (a2) and (b2) shows direction of lines scratched on graphene surface since they are hardly visible in the topographic images. In parts (c2), only two first lines are denoted by arrow, since subsequent scratched lines are clearly visible. (A colour version of this figure can be viewed online.)

$F_{N,\max}$ is the maximal force in the considered experiment. Normalized wear depth is calculated as $d = D/D_{\max}$, where D is the actual wear depth, whereas $D_{\max}$ is the maximal wear depth in the considered experiment. This normalization was introduced due to the following reasons. Although the applied normal force was used to quantify the strength of the interaction between AFM tip and substrate, the same normal force does not always give the same wear depth since the applied stress (the contact pressure or the applied normal force divided by the area over which the force is applied) is an invariant of this interaction. The contact pressure can be different for the same normal force due to the following two reasons: 1. different probes with inevitably slightly different shapes were employed for AFM scratching, and 2. due to wear of AFM probes during scratching experiments, which leads to continuous change of AFM tip shape, mostly to its flattening. As a result, due to variable area over which the normal force is applied, the same normal load could produce different stress and consequently different wear depth. The normalization of the force and wear depth was then employed to make straightforward comparison between different experiments.

Points in the graph from Fig. 7 can be grouped into three areas. The first area (I) with $d_{gr} \approx 0$ corresponds to the perfect wear protection provided by thicker graphene flakes (d_{gr} stands for the wear on graphene covered SiO_2 substrate). For high enough normal load $f = 1$, even thick graphene flakes were torn, so the wear depth in this case can take any value in the interval $0 \leq d \leq 1$ (this corresponds to partial or complete peeling of few layer graphene, or complete peeling of few layer graphene in combination with subsequent scratching of uncovered substrate, as shown in Fig. 6(c)). The second area (II) corresponds to the increased mechanical load capacity provided by thin graphene flakes. Here, the wear depths on graphene covered substrate are finite $d_{gr}>0$, and at the same

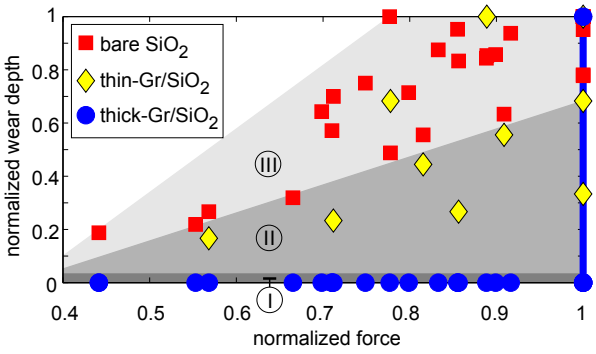

Fig. 7. Normalized wear depth d as a function of normalized force f. Three areas correspond to the following processes: (I) perfect wear protection by thick graphene flakes (blue circle), (II) increased mechanical capacity of underlying substrate provided by thin graphene flakes (yellow rhombus), and (III) wear of bare substrate (red square). Points in the figure are taken from the experimental results given in Figs. 4–6 as well as in Figs. S6 and S7 in the Supplementary material. Yellow markers in region III correspond to the case when graphene does not provide any enhancement of mechanical load capacity. Thick (blue) line for $f = 1$ (connecting blue circular markers) denotes that all wear depths are possible which corresponds to the partial or complete peeling of thick graphene flakes in a combination with subsequent plowing of uncovered substrate, as shown in Fig. 6(c). (A colour version of this figure can be viewed online.)

time $d_{gr} < d_{SiO_2}$, where d_{SiO_2} denotes the wear depth on bare SiO_2. The third area (III) corresponds to the wear on bare SiO_2 substrate. This area contains also several points where $d_{gr} > d_{SiO_2}$, showing that thin graphene flakes can not always increase the mechanical load capacity od underlying substrate.

Thin graphene, single and bilayer, can not provide wear protection. During scratching of such graphene, its properties are dominantly described with the in-plane σ-bonds. They make graphene the stiffest material, but during AFM scratching this only increases the mechanical load capacity. The wear protection requires several nanometers thick graphene. In this case, its properties during scratching are mostly determined by π-bonds between adjacent graphene layers. These bonds are responsible for weak van der Waals forces between layers. They enable easy shearing of graphene layers, and provide the interlayer repulsion when the distance between them tends to decrease. The latter property enables wear protection by few layer graphene [35]. When AFM tip scratch the surface of multilayer graphene, it deforms top graphene surface, and then this deformation is carried to inner graphene layers. As normal load increases, it tends to push adjacent graphene layers closer to each other which is then prevented by the repulsive van der Waals interaction, protecting both graphene and underlying substrate from mechanical wear.

6. Conclusion

In summary, we explain the mechanism of graphene wear at the nanoscale, the resulting change in the graphene friction, as well as the necessary conditions for wear protection by graphene. We show that the plastic deformation of graphene increases with applied normal force and inevitably leads to formation of defects in graphene lattice. For high enough normal loads, the breaking strength of graphene drops down, leading to a sudden fracture, an uncontrolled tearing and subsequent peeling off, approximately within the scratching area. In this context, scanning tunneling and tip enhanced Raman spectroscopy could be used in future studies, for imaging and understanding of atomic defects formed due to plastic deformation of graphene.

Graphene can be used as a coating for friction reduction as long as it is plastically deformed. For wear protection of the underlaying substrate, at least 5 nm thick graphene flakes are necessary. Here the repulsive van der Waals interaction between adjacent graphene layers acts as an airbag preventing wear of both graphene and underlying substrate. Extremely large stiffness of thin graphene can be employed for enhancing the mechanical load capacity of underlying substrate. Here we gave only an approximate prerequisite for the wear protection, but the efficiency of graphene films for wear protection as a function of number of graphene layers stays an open question for future studies.

Acknowledgement

This work is supported by the Serbian Ministry of Education, Science and Technological Development under Project No. OI171005 and by Qatar National Research Fund through Project NPRP 7-665-1-125. B. V. acknowledges the support by COST Action MP1303.

Appendix A. Supplementary data

Supplementary data related to this article can be found at http://dx.doi.org/10.1016/j.carbon.2017.05.036.

References

[1] K.S. Kim, Y. Zhao, H. Jang, S.Y. Lee, J.M. Kim, K.S. Kim, et al., Large-scale pattern growth of graphene films for stretchable transparent electrodes, Nature 457 (2009) 706–710.
[2] C. Lee, X. Wei, J.W. Kysar, J. Hone, Measurement of the elastic properties and intrinsic strength of monolayer graphene, Science 321 (2008) 385–388.
[3] K.-S. Kim, H.-J. Lee, C. Lee, S.-K. Lee, H. Jang, J.-H. Ahn, et al., Chemical vapor deposition-grown graphene: the thinnest solid lubricant, ACS Nano 5 (2011) 5107–5114.
[4] J.S. Bunch, A.M. van der Zande, S.S. Verbridge, I.W. Frank, D.M. Tanenbaum, J.M. Parpia, et al., Electromechanical resonators from graphene sheets, Science 315 (2007) 490–493.
[5] C. Chen, S. Rosenblatt, K.I. Bolotin, W. Kalb, P. Kim, I. Kymissis, et al., Performance of monolayer graphene nanomechanical resonators with electrical readout, Nat. Nano 4 (2009) 861–867.
[6] A.D. Smith, F. Niklaus, A. Paussa, S. Vaziri, A.C. Fischer, M. Sterner, et al., Electromechanical piezoresistive sensing in suspended graphene membranes, Nano Lett. 13 (2013) 3237–3242.
[7] S.-H. Bae, Y. Lee, B.K. Sharma, H.-J. Lee, J.-H. Kim, J.-H. Ahn, Graphene-based transparent strain sensor, Carbon 51 (2013) 236–242.
[8] S.-E. Zhu, M. Krishna Ghatkesar, C. Zhang, G.C.A.M. Janssen, Graphene based piezoresistive pressure sensor, Appl. Phys. Lett. 102 (2013) 161904.
[9] A.D. Smith, F. Niklaus, A. Paussa, S. Schröder, A.C. Fischer, M. Sterner, et al., Piezoresistive properties of suspended graphene membranes under uniaxial and biaxial strain in nanoelectromechanical pressure sensors, ACS Nano 10 (2016) 9879–9886.
[10] K.M. Milaninia, M.A. Baldo, A. Reina, J. Kong, All graphene electromechanical switch fabricated by chemical vapor deposition, Appl. Phys. Lett. 95 (2009) 183105.
[11] P. Li, Z. You, T. Cui, Graphene cantilever beams for nano switches, Appl. Phys. Lett. 101 (2012) 093111.
[12] A. Klemenz, L. Pastewka, S.G. Balakrishna, A. Caron, R. Bennewitz, M. Moseler, Atomic scale mechanisms of friction reduction and wear protection by graphene, Nano Lett. 14 (2014) 7145–7152.
[13] D. Berman, A. Erdemir, A.V. Sumant, Few layer graphene to reduce wear and friction on sliding steel surfaces, Carbon 54 (2013) 454–459.
[14] S. Tsoi, P. Dev, A.L. Friedman, R. Stine, J.T. Robinson, T. Reinecke, et al., van der Waals Screening by Single-Layer Graphene and Molybdenum Disulfide, ACS Nano 8 (2014) 12410–12417.
[15] J.S. Bunch, S.S. Verbridge, J.S. Alden, A.M. van der Zande, J.M. Parpia, H.G. Craighead, et al., Impermeable atomic membranes from graphene sheets, Nano Lett. 8 (2008) 2458–2462.
[16] S. Chen, L. Brown, M. Levendorf, W. Cai, S.-Y. Ju, J. Edgeworth, et al., Oxidation resistance of graphene-coated Cu and Cu/Ni alloy, ACS Nano 5 (2011) 1321–1327.
[17] D. Prasai, J.C. Tuberquia, R.R. Harl, G.K. Jennings, K.I. Bolotin, Graphene: corrosion-inhibiting coating, ACS Nano 6 (2012) 1102–1108.
[18] N.T. Kirkland, T. Schiller, N. Medhekar, N. Birbilis, Exploring graphene as a corrosion protection barrier, Corros. Sci. 56 (2012) 1–4.
[19] D. Berman, S.A. Deshmukh, S.K.R.S. Sankaranarayanan, A. Erdemir, A.V. Sumant, Extraordinary macroscale wear resistance of one atom thick graphene layer, Adv. Funct. Mater 24 (2014) 6640–6646.
[20] D. Marchetto, C. Held, F. Hausen, F. Wählisch, M. Dienwiebel, R. Bennewitz,

Friction and wear on single-layer epitaxial graphene in multi-asperity contacts, Tribol. Lett. 48 (2012) 77–82.
[21] F. Wählisch, J. Hoth, C. Held, T. Seyller, R. Bennewitz, Friction and atomic-layer-scale wear of graphitic lubricants on SiC(0001) in dry sliding, Wear 300 (2013) 78–81.
[22] M.-S. Won, O.V. Penkov, D.-E. Kim, Durability and degradation mechanism of graphene coatings deposited on Cu substrates under dry contact sliding, Carbon 54 (2013) 472–481.
[23] C.S. Ruiz-Vargas, H.L. Zhuang, P.Y. Huang, A.M. van der Zande, S. Garg, P.L. McEuen, et al., Softened elastic response and unzipping in chemical vapor deposition graphene membranes, Nano Lett. 11 (2011) 2259–2263.
[24] G.-H. Lee, R.C. Cooper, S.J. An, S. Lee, A. van der Zande, N. Petrone, et al., High-strength chemical-vapor-deposited graphene and grain boundaries, Science 340 (2013) 1073–1076.
[25] H.I. Rasool, C. Ophus, W.S. Klug, A. Zettl, J.K. Gimzewski, Measurement of the intrinsic strength of crystalline and polycrystalline graphene, Nat. Commun. 4 (2013) 2811.
[26] A.J.M. Giesbers, U. Zeitler, S. Neubeck, F. Freitag, K.S. Novoselov, J.C. Maan, Nanolithography and manipulation of graphene using an atomic force microscope, Solid State Commun. 147 (2008) 366–369.
[27] S. Eilers, J.P. Rabe, Manipulation of graphene within a scanning force microscope, Phys. Status Solidi B 246 (2009) 2527–2529.
[28] B. Vasić, M. Kratzer, A. Matković, A. Nevosad, U. Ralević, D. Jovanović, et al., Atomic force microscopy based manipulation of graphene using dynamic plowing lithography, Nanotechnology 24 (2013) 015303.
[29] L.-Y. Lin, D.-E. Kim, W.-K. Kim, S.-C. Jun, Friction and wear characteristics of multi-layer graphene films investigated by atomic force microscopy, Surf. Coat. Tech. 205 (2011) 4864–4869.
[30] B. Vasić, A. Zurutuza, R. Gajić, Spatial variation of wear and electrical properties across wrinkles in chemical vapour deposition graphene, Carbon 102 (2016) 304–310.
[31] A. Vasić, B. Matković, R. Gajić, I. Stanković, Wear properties of graphene edges probed by atomic force microscopy based lateral manipulation, Carbon 107 (2016) 723–732.
[32] Y. Qi, J. Liu, J. Zhang, Y. Dong, Q. Li, Wear resistance limited by step edge failure: the rise and fall of graphene as an atomically-thin lubricating material, ACS Appl. Mater. Interfaces 9 (2017) 1099–1106.
[33] E.J. Sandoz-Rosado, O.A. Tertuliano, E.J. Terrell, An atomistic study of the abrasive wear and failure of graphene sheets when used as a solid lubricant and a comparison to diamond-like-carbon coatings, Carbon 50 (2012) 4078–4084.
[34] A.V. Khomenko, N.V. Prodanov, Molecular dynamics of cleavage and flake formation during the interaction of a graphite surface with a rigid nano-asperity, Carbon 48 (2010) 1234–1243.
[35] M.M. van Wijk, A. Fasolino, Minimal graphene thickness for wear protection of diamond, AIP Adv. 5 (2015) 017117.
[36] T.-H. Fang, T.H. Wang, J.-C. Yang, Y.-J. Hsiao, Mechanical characterization of nanoindented graphene via molecular dynamics simulations, Nanoscale Res. Lett. 6 (2011) 481.
[37] W.-Y. Chang, T.-H. Fang, C.-I. Weng, J.-C. Yang, Mechanical characterizations and interface dynamics of nanoscratched graphene using molecular dynamics, J. Comput. Theor. Nanosci. 10 (2013) 832–837.
[38] C. Martin-Olmos, H.I. Rasool, B.H. Weiller, J.K. Gimzewski, Graphene MEMS: AFM probe performance improvement, ACS Nano 7 (2013) 4164–4170.
[39] F. Hui, P. Vajha, Y. Shi, Y. Ji, H. Duan, A. Padovani, et al., Moving graphene devices from lab to market: advanced graphene-coated nanoprobes, Nanoscale 8 (2016) 8466–8473.
[40] N. Severin, M. Dorn, A. Kalachev, J.P. Rabe, Replication of single macromolecules with graphene, Nano Lett. 11 (2011) 2436–2439.
[41] A. Matković, B. Vasić, J. Pešić, J. Prinz, I. Bald, A. Milosavljević, et al., Enhanced structural stability of DNA origami nanostructures by graphene encapsulation, New J. Phys. 18 (2016) 025016.
[42] D. Berman, A. Erdemir, A.V. Sumant, Graphene: a new emerging lubricant, Mater. Today 17 (2014) 31–42.
[43] C. Lee, Q. Li, W. Kalb, X.-Z. Liu, H. Berger, R.W. Carpick, et al., Frictional characteristics of atomically thin sheets, Science 328 (2010) 76–80.
[44] H. Lee, N. Lee, Y. Seo, J. Eom, S. Lee, Comparison of frictional forces on graphene and graphite, Nanotechnology 20 (2009) 325701.
[45] T. Filleter, J.L. McChesney, A. Bostwick, E. Rotenberg, K.V. Emtsev, T. Seyller, et al., Friction and dissipation in epitaxial graphene films, Phys. Rev. Lett. 102 (2009) 086102.
[46] P. Egberts, G.H. Han, X.Z. Liu, A.T.C. Johnson, R.W. Carpick, Frictional behavior of atomically thin sheets: hexagonal-shaped graphene islands grown on copper by chemical vapor deposition, ACS Nano 8 (2014) 5010–5021.
[47] S. Kwon, J.-H. Ko, K.-J. Jeon, Y.-H. Kim, J.Y. Park, Enhanced nanoscale friction on fluorinated graphene, Nano Lett. 12 (2012) 6043–6048.
[48] Q. Li, X.-Z. Liu, S.-P. Kim, V.B. Shenoy, P.E. Sheehan, J.T. Robinson, et al., Fluorination of graphene enhances friction due to increased corrugation, Nano Lett. 14 (2014) 5212–5217.
[49] J.-H. Ko, S. Kwon, I.-S. Byun, J.S. Choi, B.H. Park, Y.-H. Kim, et al., Nanotribological properties of fluorinated, hydrogenated, and oxidized graphenes, Tribol. Lett. 50 (2013) 137–144.
[50] G. Fessler, B. Eren, U. Gysin, T. Glatzel, E. Meyer, Friction force microscopy studies on SiO_2 supported pristine and hydrogenated graphene, Appl. Phys. Lett. 104 (2014) 041910.
[51] H. Chen, T. Filleter, Effect of structure on the tribology of ultrathin graphene and graphene oxide films, Nanotechnology 26 (2015) 135702.
[52] Y. Peng, Z. Wang, K. Zou, Friction and wear properties of different types of graphene nanosheets as effective solid lubricants, Langmuir 31 (2015) 7782–7791.
[53] D.K. Hong, S.A. Han, J.H. Park, S.H. Tan, N. Lee, Y. Seo, Frictional force detection from lateral force microscopic image using a Si grating, Colloids Surf. A Physicochem. Eng. Asp. 313–314 (2008) 567–570.
[54] J.H. Warner, E.R. Margine, M. Mukai, A.W. Robertson, F. Giustino, A.I. Kirkland, Dislocation-driven deformations in graphene, Science 337 (2012) 209–212.
[55] H.C. Schniepp, K.N. Kudin, J.-L. Li, R.K. Prud'homme, R. Car, D.A. Saville, et al., Bending properties of single functionalized graphene sheets probed by atomic force microscopy, ACS Nano 2 (2008) 2577–2584.
[56] K. Xu, P. Cao, J.R. Heath, Scanning tunneling microscopy characterization of the electrical properties of wrinkles in exfoliated graphene monolayers, Nano Lett. 9 (2009) 4446–4451.
[57] S.-M. Lee, J.-H. Kim, J.-H. Ahn, Graphene as a flexible electronic material: mechanical limitations by defect formation and efforts to overcome, Mater. Today 18 (2015) 336–344.
[58] H. Hiura, T.W. Ebbesen, J. Fujita, K. Tanigaki, T. Takada, Role of sp^3 defect structures in graphite and carbon nanotubes, Nature 367 (1994) 148–151.
[59] A. Zandiatashbar, G.-H. Lee, S.J. An, S. Lee, N. Mathew, M. Terrones, et al., Effect of defects on the intrinsic strength and stiffness of graphene, Nat. Commun. 5 (2014) 3186.